Introducing Adaptive Variable Friction Base Isolation Systems

Sarah Bergquist[1], Paolo Calvi[2], Richard Wiebe[2]

[1] Master's Student, Dept. of Civil and Environmental Engineering, University of Washington – Seattle, WA, USA.
[2] Professor, Department of Civil and Environmental Engineering, University of Washington – Seattle, WA, USA.

ABSTRACT

Previous research suggests that variable friction base isolation systems (VFSs) are a viable solution that can be used to protect structures against the effects of strong earthquakes. This paper introduces a new VFS device, referred to as the adaptive VFS (AVFS), which has the capability to adapt its response as a function of ground motion intensity.

The paper is organized in three parts. First, the mechanics and theoretical development of the AVFS are discussed alongside the results of a parametric study. Second, a direct displacement-based design (DDBD) process is developed for single degree of freedom (SDOF) structures. A closed-form damping equation based on a classic Jacobsen approach is derived for use in the design process; this equation is then validated using the results of over 600,000 non-linear time history analyses (NLTHA). Lastly, preliminary validation of the DDBD process for both rigid and flexible SDOF structures is conducted. Realistic AVF devices are designed considering input response spectra associated with five cities on the West Coast of the US for two different return periods. The results of the analyses indicate that for the SDOF case study structures studied, the proposed DDBD process is effective at predicting the behavior of the AVFS for all earthquake intensity levels considered. This study shows promise for extension into multiple degree of freedom (MDOF) structures.

Key words: Base isolation, variable friction systems, friction pendulum, adaptive-response, performance-based design

INTRODUCTION

The use of sliding isolation devices, such as friction pendulum systems (FPSs), have been shown to be effective in mitigating seismic effects on both buildings and bridges [1]. The devices are particularly valuable because they can control force transferred to the superstructure through careful design of stiffness and displacement capacity. FPSs are capable of being designed for one demand level, but with the increasing acceptance of performance-based design (PBD) in engineering practice, it is becoming common to seek to control a structure's response for two or more demand levels.

As a part of recent studies, a new family of friction-based isolation devices, referred to as variable friction systems, was introduced [2-4]. Through different combinations of ring size and friction coefficients, it is possible to produce more desirable hysteretic responses, as seen in Figure 1. For example, for the same displacement demand, VFS devices like the BowTie and BowC exhibit higher energy dissipation properties when compared to equivalent FPSs [3]. Much remains to be explored regarding variations of VFS, including how it can be used to encompass PBD objectives.

The AVFS is one of the many possibilities of VFS adaption for PBD. This device behaves as an FPS for design-level demands, but stiffens when that displacement demand is exceeded, likely from a rare event. This adaptability of behavior allows designers to have control over the behavior of the device, and therefore the structure, for multiple earthquake intensities [5]. Without adaptability, a designer who wanted an FPS capable of taking the demand of a rare event would have to allow for increased force transferred to the structure during smaller events.

AVFS properties are studied through development of the device's mechanics, determining numerical modeling methods, and performing a parametric study using a customized one-dimensional analysis program in Matlab [6]. The parametric study is used to help inform the design method. Guidelines for a DDBD process are proposed for both rigid and flexible SDOF systems, which uses a derived and preliminarily validated damping expression. Designs for both flexible and rigid SDOF systems are compared to NLTHA, which is used to draw conclusions about the design methodology and the ability to predict the behavior of AVFSs. The properties and application of AVFSs has not been extensively studied before; thus, this paper serves as a preliminary exploration into the potential of AVF devices, and more in-depth work should be done.

MECHANICS

Adaptive Variable Friction Device

The AVF device, shown in Figure 1, has re-centering properties similar to an FPS, and can adapt to resist large seismic events. The device's lateral resistance comes from both curvature and friction; when added in parallel, the AVFS hysteresis is created, as seen in Figure 2. Similar to an FPS, the AVFS consists of a fixed-base stainless steel spherical cap defined by radius of curvature R. Concentric rings on the spherical cap are defined by two friction and displacement values: the friction coefficients, μ_1 and μ_2 (note, $\mu_1 < \mu_2$), correspond to the inner and outer ring, and the displacement demands, Δ_{DBE} and Δ_{MCE}, correspond to DBE and MCE design levels which have return periods of 475 and 2475 years, respectively. Note, these demands can be changed to meet other performance goals. An articulating slider of radius r_s is free to move throughout the device and is made using a low-friction material, such as polytetrafluorethylene [2]. The slider moves over the stainless steel base, which is treated to obtain the desired friction coefficients. Note that the difference between Δ_{MCE} and Δ_{DBE} should be made equal to or less than the diameter of the slider since the hysteretic behavior changes if the slider moves past this displacement, shown in Figure 2.

Force Displacement Relationship

The lateral force-displacement relationship for an AVFS device can be seen in Figure 1. For this discussion, it is assumed that the axial stress is uniform over the slider area, that there is no difference between static and dynamic friction, and that friction is well defined and perfectly stable.

An AVF system has a perfectly rigid response until the device is activated at V_0, or the weight times the first friction coefficient. Once the device is activated, the slider begins to move with respect to the bottom fixed plate, with lateral resistance coming from the area of the slider on the first ring (Figure 1b). As the slider transitions to the outer ring, the lateral resistance comes from both rings, proportional to the overlapping areas times the appropriate friction coefficients (Figure 1c). This transition, defined in mathematical detail in [4], is nonlinear depending on the sizes of the rings and their friction properties. When the load is reduced and reversed, the device will exhibit a perfectly rigid response until it is activated in the opposite direction, which happens at a value that depends on the shape of the hysteresis and is determined in the design process. After activation, the lateral load required to push the slider back decreases then increases as it moves from the outer ring to the inner ring, then to the outer ring on the other side (Figure 1d). The force-displacement curve is rotationally symmetric about the origin and therefore exhibits the same response as quadrant IV of Figure 1d when returning back to the center (Figure 1e).

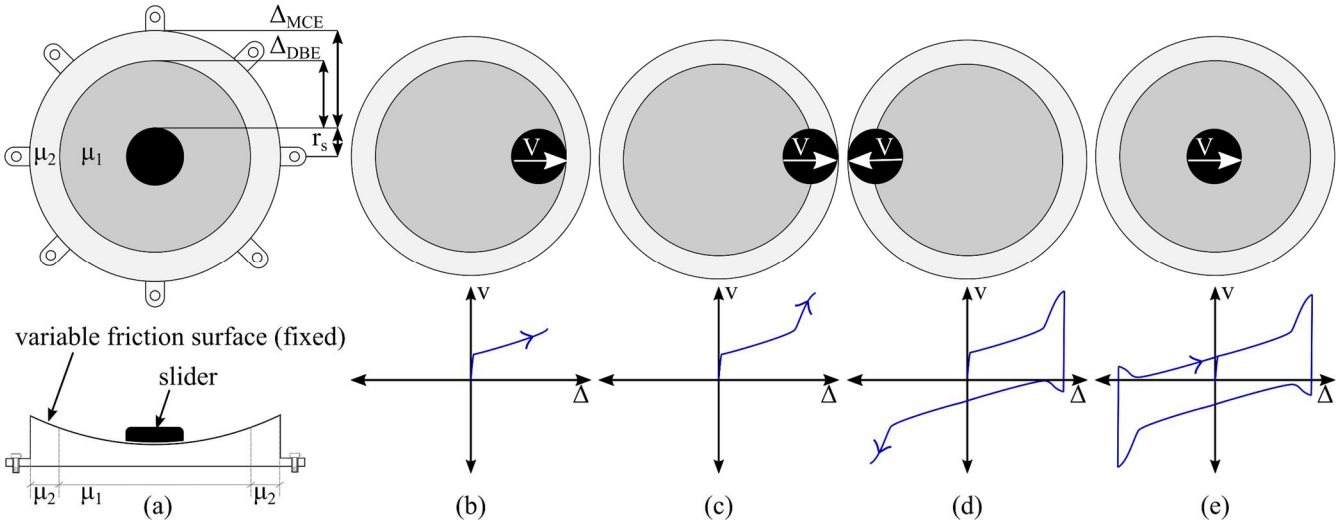

Figure 1. (a) Cross-sectional and aerial view of an AVFS device, (b) Force-displacement response of AVFS at post-activation, (c) at maximum displacement, (d) at lateral load reversal, and (e) returned to initial position.

Numerical Modeling

In order to study the AVFS device, a numerical model was developed to compute structural excitations resulting from input ground motions. Though the actual force functions of the AVFS are nonlinear, the hysteresis is idealized as a piece-wise linear function as shown in Figure 2; it should be noted that this work should be expanded on using the exact model, such as the one developed in [7]. The initial stiffness K_0 should ideally be considered rigid, but is modeled as 10,000 times the post activation stiffness for numerical convergence reasons, and is exaggerated in Figure 2 for visualization purposes. From a small sensitivity study, such a large initial stiffness has been shown to not affect analysis results. Additionally, K_0's contribution to the post activation stiffness, K_1, is negligible when added in series and is therefore neglected in K_1's calculation.

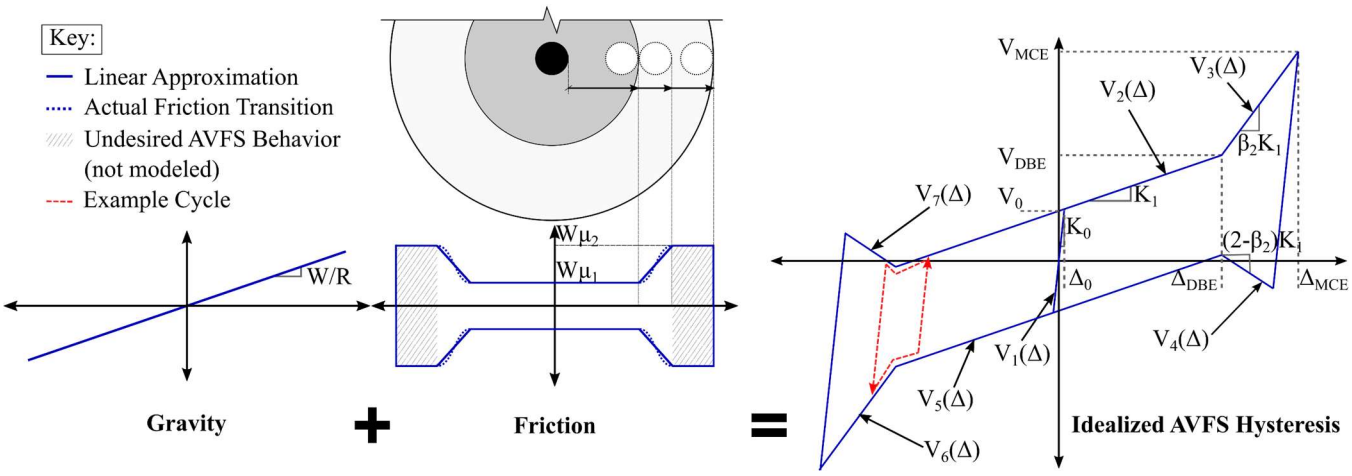

Figure 2. Components of Hysteresis and Idealized Hysteretic Response of AVFSs used for Numerical Modeling

In order to model the AVFS hysteretic shape, the translational DOF of the structure was replaced with a nonlinear spring defined using Eq. (1) - an application of the lumped plasticity approach. The modeling was based entirely on mechanical considerations, however more complex models are being developed in accordance with experimental data which naturally incorporates thermal and degradation effects [7]. In order to fully define the hysteretic behavior of an AVFS for NLTHA, the following parameters must be provided:

Table 1. AVFS Parameters Needed to Define NLTHA

Name	Symbol	Computation
Seismic Weight	W	User-defined
Radius of Curvature	R	From design process
First Friction	μ_1	User-defined
Design Displacement	Δ_{DBE}	User-defined
Activation Displacement	Δ_0	V_0/K_0
Design Force	V_{DBE}	From design process
Activation Force	V_0	$W\mu_1$
Post-activation Stiffness	K_1	W/R
Initial Stiffness	K_0	~10,000K_1
Adaptive Stiffness Coefficient	β_2	User-defined

The backbone and unloading/reloading curves combine to give the final hysteretic response according to:

$$V(\Delta) = \begin{cases} max[min(V_1(\Delta), V_2(\Delta)), V_5(\Delta)] & if\ -\Delta_{DBE} \le \Delta \le \Delta_{DBE} \\ max[min(V_1(\Delta), V_3(\Delta)), V_4(\Delta)] & if\ \Delta > \Delta_{DBE} \\ max[min(V_1(\Delta), V_7(\Delta)), V_6(\Delta)] & if\ \Delta < -\Delta_{DBE} \end{cases} \quad (1)$$

The linear approximation of AVFS hysteretic behavior can be expressed as:

$$\begin{aligned} V_1(\Delta) &= K_0(\Delta - \Delta_p) \\ V_2(\Delta) &= V_0 + K_1\Delta \\ V_3(\Delta) &= V_0 + K_1\Delta_{\mathrm{DBE}} + \beta_2 K_1(\Delta - \Delta_{\mathrm{DBE}}) \\ V_4(\Delta) &= -V_0 + K_1\Delta_{\mathrm{DBE}} + (2-\beta_2)K_1(\Delta - \Delta_{DBE}) \\ V_5(\Delta) &= -V_0 + K_1\Delta \\ V_6(\Delta) &= -V_0 - K_1\Delta_{\mathrm{DBE}} + \beta_2 K_1(\Delta + \Delta_{DBE}) \\ V_7(\Delta) &= V_0 - K_1\Delta_{\mathrm{DBE}} + (2-\beta_2)K_1(\Delta + \Delta_{DBE}) \end{aligned} \quad (2)$$

where Δ_p represents the plastic offset calculated at each converged stage of the analysis, and is defined as:

$$\Delta_p = \Delta - \Delta_0 \quad (3)$$

The analysis program for this study, written in Matlab [6], uses linear acceleration Newmark-Beta algorithm for integration [8] and uses Newton-Raphson methods to calculate the secant stiffness of the system.

Parametric Study

In order to characterize the AVF device, a preliminary parametric study was conducted. The parameter ranges studied, found in Table 2, reflect the displacements and radii of curvature currently used by base isolation manufacturers. Friction coefficient ranges are limited by material technology; however, large, and therefore currently unrealistic values of μ_2, characterized by β_2, were included in the study in order to see a fuller range of behavior of the AVFS. Note, $\beta_2 = 1$ is equivalent to an FPS and was included for comparison.

Table 2. Parameters Studied (Low:Step:High)

R [m]	β_2	Δ_{DBE} [m]	μ_1 [%]	**Ground Motion Scale Factor**
1.5:0.5:5	1:1:5,7,9	0.1:0.1:0.5	3,5,8	0.5:0.5:2.5

The horizontal components of 10 ground motions (i.e. 20 total) scaled to San Francisco's DBE and MCE response spectra were used in the SDOF NLTHA. Note, the ground motion scale factor in the parametric study is in addition to the scaling factor used to match the response spectra. The weight of the superstructure was normalized and assigned both an infinite stiffness and damping of 0% in order to study only the isolator properties.

In order to show five parameters graphically, three test matrices were created, one for each μ_1.The full graphical representation of the results is quite large, so a representative portion for a ground motion scale factor of 2 and a μ_1 of 5% is shown in Figure 3. Each test matrix consisted of subplots organized by increasing Δ_{DBE} (horizontal) and scale factor (vertical). Each individual subplot shows the average of the response parameter of interest (maximum displacement, maximum force, and absolute residual displacement) for all ground motions plotted as a function of β_2 against R. The combination of the five parameters and ground motions resulted in over 80,000 NLTHAs.

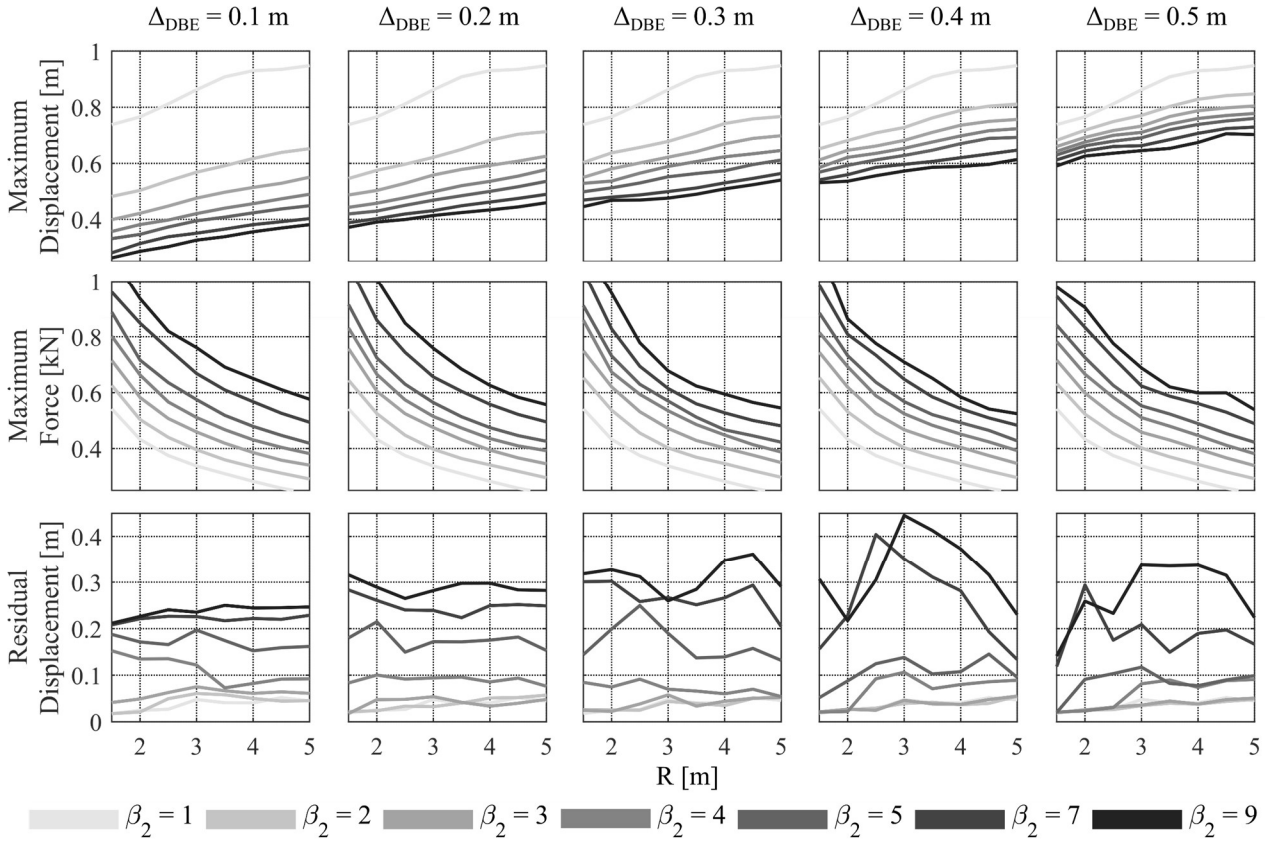

Figure 3. Parametric Study Results for Scale Factor = 2, μ_1 = 5%

It is apparent that the maximum displacement decreases with increasing β_2, which makes sense since an increased μ_2 results in a higher force over a shorter distance. However, since there is a trade-off between force and displacement, devices with higher β_2 on average have higher maximum forces and residual displacements for all R and Δ_{DBE} values. If re-centering is important to a designer, then devices with lower β_2 values would be advantageous.

An AVFS shows potential advantage over FPSs when maximum displacement and force are compared. When comparing β_2 = 1 and 2, the difference between the maximum displacement is much larger than the difference between maximum force,

implying that an AVFS with $\beta_2 = 2$ is capable of achieving a similar low maximum force as an FPS, but with lower displacement demand. This could be important for designers constrained by displacement. Additionally, β_2 values ≤ 3 have small absolute residual displacements for all R and Δ_{DBE} values, giving them similar re-centering properties to the FPS. If re-centering is very important to the designer, designing a device with $\alpha_1 \geq 2$ and $\beta_2 = 2$ allows for low residual displacement. This was tested in a small study by increasing the scale factor to 20 and evaluating the residual displacement. This knowledge of the relationship between friction, curvature, and β_2 influenced the design of devices, discussed in the next section.

AVFS DESIGN PROCESS FOR SDOF SYSTEMS

It is recommended by Calvi et al. [2-4] that the direct displacement-based design method developed by Priestly et al. [9] be implemented for variable friction systems. This design method has already been adapted for various VFSs such as the BowTie and BowC [4] and was adapted further for this AVFS design process. Figure 5 shows the design process for flexible SDOF structures; to adapt for a rigid system, set the structure's damping and DBE design displacement to zero.

There are two parts to the AVFS design process: Part 1) friction pendulum design for DBE demand levels, denoted in blue in Figure 5, and Part 2) the adaptive design for MCE demand levels, denoted in red. In Part 1 of the process, the designer chooses α_1 (the ratio between the DBE and activation shear), the structure and isolator displacement at DBE level, and assigns the structure's elastic damping. From there, the system displacement at DBE demand can be calculated, along with the isolator and system damping (Eq. (4) - (6)) [3, 9]. The DBE displacement spectrum is then reduced, which can be done either by using the Eurocode reduction factor shown in Eq. (7) as done by Timsina for BowTie and BowC design [3], or by creating a response spectrum with the given damping (more accurate). An effective system period at the DBE level is found from the reduced spectrum, and a corresponding effective stiffness is calculated (Eq. (8), (9)). Next, the DBE shear is calculated by multiplying the effective stiffness with the system displacement; then, corresponding parameters like the activation force, R, and μ_1 can be calculated (Eq. (10) - (13)). Finally, the structural stiffness required to meet the DBE demand is then calculated using Eq. (14).

Part 2, or the adaptive design, begins with choosing the slope of the adaptive branch via β_2. From the parametric study, it was shown that β_2 has a large effect on maximum displacement, force, and residual displacement. When β_2 is larger, there is a higher chance of a device "getting stuck," or having a large residual displacement. Therefore, control over the slope is given so that the designer can balance the trade-off between higher force resistance and higher residual displacement. Once the slope is chosen, there is only one corresponding MCE demand, which can be found through iteration. Each iteration begins with the MCE displacement being calculated for a given γ, defined as the ratio of MCE to DBE displacement (Eq. (15)). The MCE shear demand can be calculated using Eq. (16), and corresponding ratio between MCE and DBE shears, α_2, can be found using Eq. (17). The damping of the AVF isolator can be found using Eq. (18), which is discussed in the next section. Eq. (10) can be used to find the MCE effective stiffness, and Eq. (9) to find the corresponding MCE effective period. Using the MCE structure and isolator displacements, the system damping is found using Eq. (6) which is then used to calculate an MCE displacement demand (Eq. (19)) based on the reduced MCE spectrum. If the two MCE displacements from Eq. (15) and (19) are equal, the designer can continue to calculate the second friction coefficient (Eq. (20), (21)). The design is complete if the forces and displacements meet the desired performance objectives and the radius of curvature and friction coefficients can be manufactured.

Equivalent Viscous Damping Validation

Damping of VFSs has previously been represented using Equivalent Viscous Damping (EVD) [2], which is based on Jacobsen's equivalence between the energy dissipated in a cycle of the system and the energy dissipated by an equivalent viscous system [10]. Eq. (18) was derived using this approach. In order to validate the expression for use in design, a suite of over 600,000 NLTHAs was conducted and compared to equivalent EVD values from Eq. (18), as shown in Figure 4. Parameter ranges for the EVD validation were similar to that of the parametric study. Overall, the averages of the analysis and equation are similar, especially for lower values of α_2. Due to the similar trends between the equation and analysis data, Eq. (18) was used in the AVFS design process. It should be noted that it may be necessary to calibrate the equation for different values of β_2 to make the damping prediction more accurate.

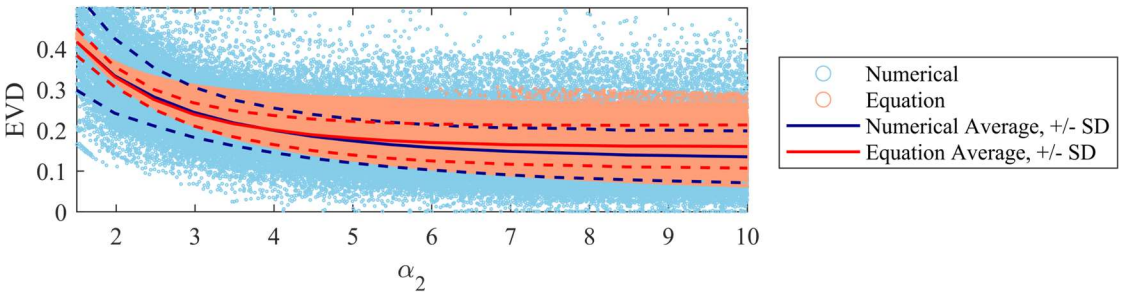

Figure 4. Equivalent Viscous Damping of AVFS

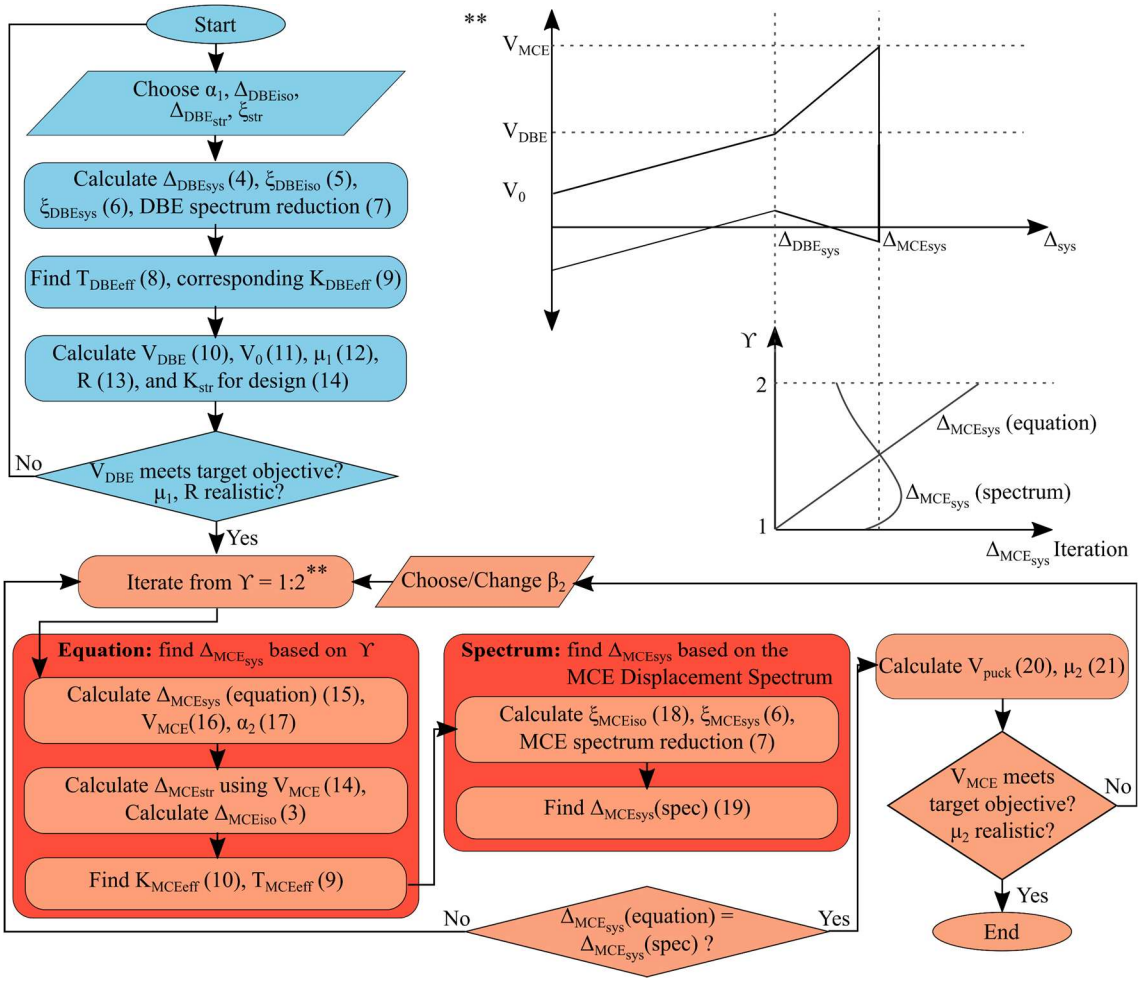

$$\Delta_{sys} = \Delta_{str} + \Delta_{iso} \quad (4)$$

$$\xi_{DBE_{iso}} = 2/(\pi\alpha_1) \quad (5)$$

$$\xi_{sys} = (\xi_{str}\Delta_{str} + \xi_{iso}\Delta_{iso})/\Delta_{sys} \quad (6)$$

$$\eta = \sqrt{0.07/(0.02 + \xi_{sys})} \quad (7)$$

$$T_{eff} = T_{spec}\Delta_{sys}/(\Delta_{spec}\eta) \quad (8)$$

$$K_{eff} = 4\pi^2 m/T_{eff}^2 \quad (9)$$

$$V = K_{eff}\Delta_{sys} \quad (10)$$

$$V_0 = V_{DBE}/\alpha_1 \quad (11)$$

$$\mu_1 = V_0/W \quad (12)$$

$$R = W\Delta_{DBE_{iso}}/(V_{DBE} - V_0) \quad (13)$$

$$K_{str} = V_{DBE}/\Delta_{DBE_{str}} \quad (14)$$

$$\Delta_{MCE_{sys}}(guess) = \gamma\Delta_{DBE_{sys}} \quad (15)$$

$$V_{MCE} = V_{DBE} + \frac{\Delta_{MCE_{sys}} - \Delta_{DBE_{sys}}}{1/K_{str} + 1/(\beta_2 W/R)} \quad (16)$$

$$\alpha_2 = V_{MCE}/V_{DBE} \quad (17)$$

$$\xi_{MCE_{iso}} = \frac{2\gamma + (\alpha_2 - \alpha_1)(\gamma - 1) - (\alpha_1 - 1)(\gamma - 1)^2}{\pi\alpha_2\gamma} \quad (18)$$

$$\Delta_{MCE_{sys}}(spec) = \Delta_{spec}T_{eff}/T_{spec}\sqrt{0.07/(0.02 + \xi_{sys})} \quad (19)$$

$$V_{puck} = V_{DBE} + \beta_2(W/R)d_{puck} \quad (20)$$

$$\mu_2 = \left(V_{puck} - W/R(\Delta_{DBE_{iso}} + d_{puck})\right)/W \quad (21)$$

Figure 5. AVFS Design Flowchart and Equations for Flexible SDOF Systems

PRELIMINARY AVFS DESIGN VALIDATION

Case Study Structures

In order to test the ability of the AVFS design process to predict behavior, two sets of devices were designed for the demand of 5 different US cities: one set for rigid structures, and one set for flexible. Each city had 20 far-field ground motions (10 pairs) except for San Francisco, which also had a set of pulse ground motions. The input parameters α_1, Δ_{DBEiso}, and β_2 (ranging from 2-5) were kept the same between the rigid and flexible designs to allow for direct comparison. The flexible structure had a damping of 5%, height of 4 m, and a DBE story drift of 1%; though this drift would most likely cause yielding in the superstructure, it was chosen in order to see the effects of a flexible structure on the accuracy of the design predictions. To eliminate sources of possible error in the validation process, the DBE and MCE demand spectra were reduced by re-calculating each ground motion's spectrum given a damping coefficient instead of using the reduction factor in Eq. (7). The pressure on the puck was 50 MPa, with a puck diameter of 0.2 m. Note, the puck diameter was increased for the San Francisco pulse devices in order to maintain bi-linear hysteretic behavior. Results of the designs are summarized in Table 3.

Table 3. AVFS Design Parameters

Rigid/Flexible			**Los Angeles**			**Portland**			**San Diego**			**San Francisco**			**San Francisco (Pulse)**			**Seattle**		
R	m	*R*	4.6	7.0	7.1	2.2	3.2	5.4	3.1	4.4	8.7	2.6	4.7	6.0	5.0	6.3	8.5	2.1	2.7	3.8
		F	4.7	7.2	7.4	2.8	3.9	6.8	3.7	6.8	12.4	2.6	4.8	6.0	5.4	7.0	8.9	2.4	3.2	4.2
μ_1	%	*R*	5.4	4.5	3.6	5.4	3.4	3.0	3.2	3.0	2.3	3.9	3.4	3.0	4.1	3.6	3.0	4.0	3.5	2.5
		F	5.4	4.3	3.4	4.3	2.7	2.3	2.7	2.0	1.6	3.8	3.3	3.0	3.8	3.2	2.9	3.6	3.0	2.3
μ_2	%	*R*	22.6	16.0	14.8	14.4	9.6	6.7	22.5	16.7	9.2	11.6	7.7	6.4	8.1	6.7	5.4	23.1	18.2	12.9
		F	22.5	15.4	14.2	11.5	7.8	5.3	18.8	10.8	6.5	11.3	7.5	6.3	7.5	6.1	5.1	20.4	15.6	11.8
Δ_{DBE}	m	*R/F*	0.25	0.31	0.38	0.12	0.16	0.16	0.20	0.20	0.20	0.20	0.24	0.27	0.31	0.34	0.38	0.17	0.19	0.24
Δ_{MCE}	m	*R*	0.41	0.47	0.55	0.22	0.29	0.29	0.30	0.32	0.36	0.33	0.43	0.49	0.52	0.58	0.65	0.27	0.29	0.37
		F	0.38	0.47	0.56	0.22	0.28	0.29	0.30	0.33	0.34	0.33	0.43	0.48	0.52	0.58	0.64	0.26	0.30	0.35
T_{sys}	sec	*R*	2.44	3.04	3.24	2.12	2.66	3.29	2.32	2.63	3.48	2.47	3.22	3.63	3.35	3.76	4.34	2.03	2.32	2.81
		F	2.77	3.37	3.57	2.74	3.34	4.15	2.90	3.73	4.77	2.77	3.56	3.93	3.72	4.20	4.69	2.50	2.84	3.30

Results

The results from all devices normalized by their respective design values can be seen in Figure 6.

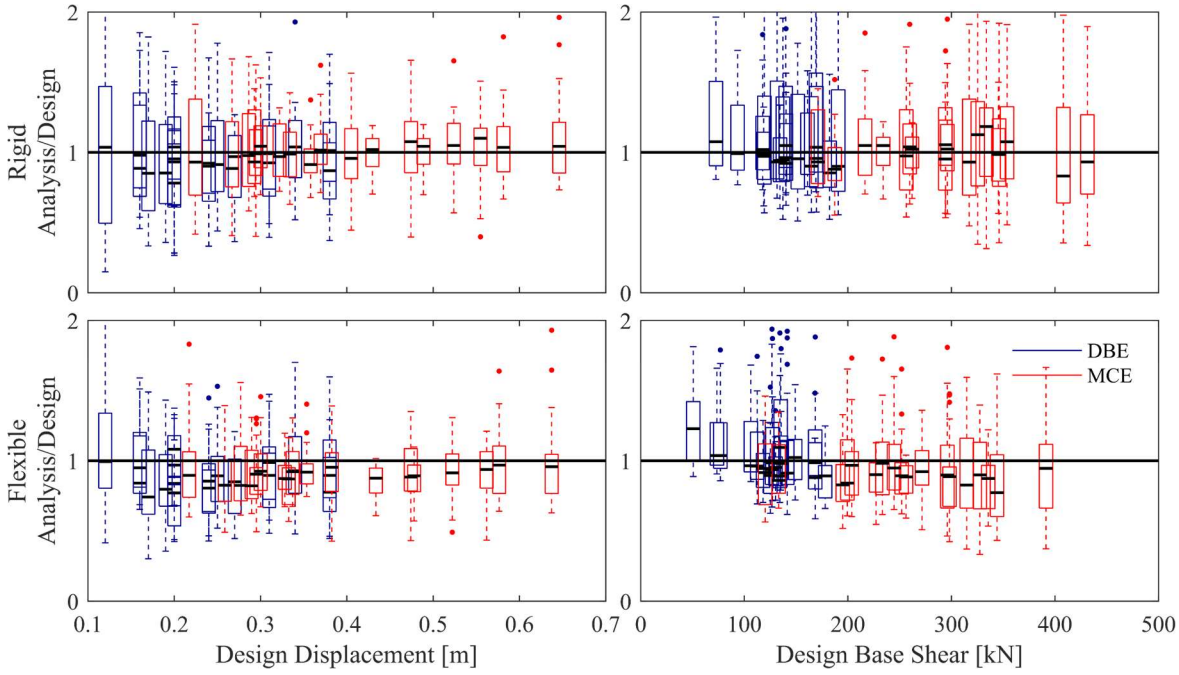

Figure 6. Design vs. NLTHA for Rigid and Flexible SDOF Systems

Each boxplot represents a device design, with the thick horizontal black line representing the mean of the 20 NLTHA for that device, the error bars showing maximum and minimum values, and the dots representing outliers. For the rigid devices, the

displacements are overall the same for the design and mean analysis. In the flexible system, overall forces and displacements from design were conservative, suggesting the system damping equation may overestimate damping. The design values for rigid structures matched analysis better than flexible, though flexible design values still predicted behavior well. This agreement between design and analysis for 36 different devices defined with different β_2 values across 5 cities shows that the design method for AVFS systems can predict behavior well for rigid and flexible SDOF systems using a simplified numerical model. Note that this agreement includes the set of pulse ground motions, which can be hard to design and predict.

The residual displacements from the NLTHA, graphed against β_2 in Figure 7 show small residual displacements for all β_2 values, making the AVFS comparable to an FPS in terms of residual displacement. Note each city had the same β_2 for design, with duplicate β_2 values for 2 cities. Though the results from this study suggest promising behavior prediction for AVFS devices, the results should be verified using more complex, real-world structural conditions.

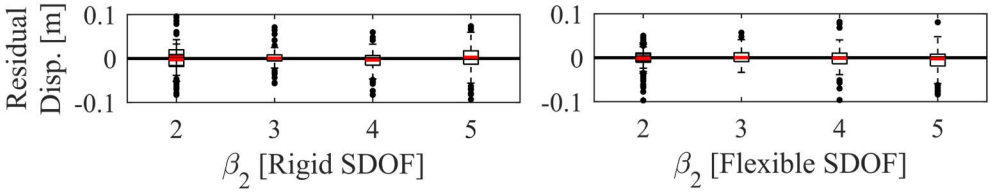

Figure 7. Residual Displacement from NLTHA for Rigid and Flexible SDOF Systems

CONCLUSIONS

This paper has introduced a new type of variable friction bearing called AVFS and explored its analysis and design. The mechanics of the device were discussed alongside suggested numerical modeling techniques for an idealized hysteresis. A parametric study showed that β_2 values ≤ 3 provide re-centering capabilities similar to an FPS and that the AVFS demonstrated an advantage over FPS in displacement capacity: for a similar maximum force, the AVFS requires a much lower maximum displacement than an FPS. A design process for SDOF systems was proposed following the framework of DDBD and analyzed using NLTHA. The force and displacement results for the rigid structures were on average in agreement with the design values, including the systems designed for pulse ground motions, and the residual displacement on average for all β_2s studied was very low, again similar to an FPS. Though the AVFS concepts presented in this paper are preliminary, the device shows promise regarding re-centering capabilities paired with an improved maximum force/displacement trade-off. The straightforward design process presented and analyzed shows that designers can have confidence in the ability to predict performance for SDOF systems, which therefore makes AVF devices a viable and effective alternative to other base isolation systems for achieving PBD objectives and improving the seismic performance of structures.

ACKNOWLEDGMENTS

The funding for this research was generously provided in part by the University of Washington's Valle Scholarship.

REFERENCES

[1] Calvi, P.M., and Calvi, G.M. (2018). "Historical development of friction based seismic isolation systems". *Soil Dynamics and Earthquake Engineering*, 106: 14-30.

[2] Calvi PM, Moratti M, Calvi GM. *Seismic Isolation Devices Based on Sliding Between Variable Friction Coefficient*. Earthquake Spectra 2016; 32(4): 2291-2315.

[3] Timsina S, Calvi PM. *Damping Properties of Variable Friction Base Isolation Systems.* 16th European Conference on Earthquake Engineering 2018, Thessaloniki, Greece.

[4] Calvi PM, Ruggiero DM. *Numerical modelling of variable friction sliding base isolators*. Bulletin of Earthquake Engineering 2016; 14(2): 549-568.

[5] Fenz DM, Constantinou MC. *Spherical sliding isolation bearings with adaptive behavior: Theory*. Earthquake Engineering and Structural Dynamics 2008; 37(2): 163-183.

[6] MATLAB R 2018A, The MathWorks, Inc., Natick, Massachusetts, United States.

[7] Yang, T., Calvi, P.M., Wiebe, R., (2019*). Numerical implementation and experimental validation of the behavior of variable friction sliding base isolators.* Earthquake Spectra. *Under review.*

[8] Newmark, N. M. and Rosenblueth, E. (1971). *Fundamentals of Earthquake Engineering*. Civil Engineering and Engineering Mechanics Series, 12.

[9] Priestley, M. J. N., et al. *Displacement-Based Seismic Design of Structures*. EUCENTRE, 2017.

[10] Jacobsen, L. S. *Damping in composite structures*. Proc. of the Second World Conference on Earthquake Engineering. Vol. 2, pp.1029–1044. Tokyo and Kyoto, Japan.